X-ray study of *M*-shell ionization of heavy atoms by 8.0–35.2-MeV O^{q+} ions: The role of the multiple-ionization effects

M. Czarnota,* D. Banaś, J. Braziewicz, J. Semaniak, and M. Pajek
Institute of Physics, Jan Kochanowski University, 25-406 Kielce, Poland

M. Jaskóła and A. Korman
The Andrzej Soltan Institute for Nuclear Studies, 05-400 Otwock-Świerk, Poland

D. Trautmann
Institut für Theoretische Physik, Universität Basel, CH-4056 Basel, Switzerland

W. Kretschmer
Physikalisches Institut, Universität Erlangen–Nürnberg, D-91058 Erlangen, Germany

G. Lapicki
Department of Physics, East Carolina University, Greenville, North Carolina 27858, USA

T. Mukoyama
Kansai Gaidai University, Hirakata, Osaka 573-1001, Japan
(Received 26 November 2008; published 19 March 2009)

The *M*-shell ionization in high-*Z* atoms by O^{q+} ions have been studied systematically in the energy range of 8.0–35.2 MeV in order to verify the available theoretical approaches describing the *M*-shell ionization by charged particles in asymmetric collisions. The measured *M* x-ray spectra were analyzed taking into account the effects of x-ray line shifting and broadening caused by the multiple ionization in the *M* and *N* shells. The *M*-subshell ionization cross sections, derived by using the *M*-shell decay rates modified for the multiple ionization effects, have been compared with the theoretical predictions based on the plane-wave Born approximation (PWBA), the semiclassical approximation (SCA), and the binary-encounter approximation (BEA). In the PWBA approach two theoretical calculations were considered: the energy-loss Coulomb deflection perturbed stationary state relativistic (ECPSSR) theory and its recent modification called the energy-loss Coulomb deflection united and separated atoms relativistic (ECUSAR) theory, which corrects a description of the electron binding effect to account for the united and separated atoms (USA) electron binding energy limits. In the SCA calculations performed with relativistic hydrogenic wave functions the binding effect was included in the limiting cases of separated-atom (SA) and united-atom (UA) limits. The measured *M*-subshell ionization cross sections are the best reproduced by the SCA-UA calculations, with exception of the $M_{2,3}(3p)$-subshell cross sections which are strongly enhanced and cannot be reproduced by the discussed calculations.

DOI: 10.1103/PhysRevA.79.032710 PACS number(s): 34.50.−s

I. INTRODUCTION

The excitation of x rays in ion-atom collisions is an important fundamental process of interaction of charged particles with matter. In asymmetric ($Z_1 \ll Z_2$) collisions, with Z_1 and Z_2 being the atomic numbers of projectile and target atom, respectively, a creation of inner-shell vacancy is dominated by the direct Coulomb ionization. The excited atoms decay radiatively by emission of x rays or nonradiatively by the Auger or Coster-Kronig processes. Consequently, the investigations of ion-induced x rays allow us to determine the ionization cross sections for ion impact, which are both of fundamental and practical interest. The experimental studies of inner-shell ionization by ions are important for testing the theoretical description of this process as well as for applications, for instance, for the particle induced x-ray emission (PIXE) technique.

In early studies concerning inner shells ionization by charged particles mainly *K* and *L*-shell ionization by light ions was investigated, which is summarized in Refs. [1–9]. The investigations of the *M*-shell ionization by observation of *M* x rays excited by ion impact are generally more difficult experimentally due to very low energies of studied *M* x rays, being typically within the range of 1–3 keV, which furthermore cannot be fully resolved by a semiconductor x-ray detector. For these reasons the results of early measurements of *M*-shell ionizations by light ions, which were done with gas proportional counters, were less accurate than the results obtained in later studies which were performed using semiconductor x-ray detectors. For accurate measurements of *M* x rays a precise efficiency calibration of x-ray semiconductor detector is necessary. Such a calibration technique, which was described in detail in Ref. [10], was used in the systematic studies of *M*-shell ionization by light ions [11–16], which were undertaken in our group. The results of these studies concerning the *M*-shell ionization by light $^{1,2}H$

*marcin@pu.kielce.pl

 ©2009 The American Physical Society

and ^{3,4}He ions were recently summarized in Ref. [17], where the references to earlier experiments on M-shell ionization by light ions can be found.

The studies of M-shell ionization by heavy ions ($Z_1 \gg 1$) [18–25] are generally much more complex, mainly, due to the multiple ionization effects and increasing role of the electron capture. In particular, the multiple ionization process affects substantially the observed x-ray spectra by *shifting* and *broadening* the M x-ray lines, which additionally complicates a resolution of individual M x-ray transitions. Moreover, the multiple ionization process influences conversion of the measured x-ray yields into the ionization cross sections by modifying the M-shell decay radiative, Auger, and Coster-Kronig yields. Additionally, the vacancy rearrangement processes, taking place between a moment of *collision* and x-ray *emission*, have to be considered. Consequently, the multiple ionization effects are very important for correct interpretation of M x-ray emission induced by energetic heavy ions. In fact, the investigations of a role of the multiple ionization effects in the M-shell ionization by heavy ions was our main motivation to study the M x-ray production and M-shell ionization cross sections of selected heavy atoms ($_{79}$Au, $_{83}$Bi, $_{90}$Th, and $_{92}$U) in collisions with oxygen ions. In contrast to previous experimental studies [18–25] on the M-shell ionization by heavy ions, in the present work the effects of multiple ionization were included in interpretation of the data which resulted, in our opinion, in a substantial improvement of a quality of the reported results.

In strongly asymmetric collisions ($Z_1 \ll Z_2$) the inner shell vacancies are created in direct Coulomb ionization process, i.e., by exciting a bound electron directly to a continuum. This process can be described theoretically within the first-order perturbation approaches, namely, the plane-wave Born approximation (PWBA) [26] and the semiclassical approximation (SCA) [27]. The direct ionization can be described using the binary-encounter approximation (BEA) [28,29], which is a nonperturbative approach based on the classical treatment of the collision. The PWBA-based approach was further extended to include the corrections for the binding and polarization effects, treated within the perturbed stationary states (PSS) approximation, as well as the Coulomb deflection, energy loss, and relativistic effects. This theory, which is known as the energy-loss Coulomb deflection perturbed stationary state relativistic (ECPSSR) theory [30], was further modified to reproduce correctly the binding effect in the united- and separated-atoms limits. In the resulting energy-loss Coulomb deflection united and separated atoms relativistic (ECUSAR) theory [31] the binding correction was saturated at the united-atoms limit. In the semiclassical SCA approach the direct ionization of a bound electron by a projectile is described within the time-dependent first-order perturbation treatment, with projectile moving on the classical trajectory. In the SCA calculations the hyperbolic projectile trajectory and relativistic electronic wave functions can be used in an exact way, while the binding effect can be treated only approximately for the extreme cases of separated atoms (SCA-SA) or united atom (SCA-UA) limits.

In the present paper the results of systematic measurements of the M-shell ionization of $_{79}$Au, $_{83}$Bi, $_{90}$Th, and $_{92}$U atoms by O^{q+} ions in the energy range of 8.0–35.2 MeV are discussed. As it is demonstrated in the paper the multiple ionization in outer M and N shells is crucial for a correct interpretation of the measured M x rays to obtain reliable M-shell ionization cross sections. The results are discussed in terms of available theoretical treatments of the direct Coulomb ionization, which are based on the basic SCA, PWBA, and BEA approaches. The paper is organized as follows. The experimental aspects of this work are described in Sec. II. In Sec. III the multiple ionization effects in the measured x-ray spectra are discussed, while the data analysis is described in Sec. IV. In Sec. V the main experimental results are presented including a discussion of a modification of the M-shell decay rates in multiply ionized atoms needed to derive the M-shell ionization cross sections. In Sec. VI the available theoretical approaches (PWBA, SCA, BEA, ECPSSR, ECUSAR) treating the M-shell ionization are described followed by a discussion of the results in Sec. VII. The paper is summarized in Sec. VIII.

II. EXPERIMENT

In the present experiment oxygen ions of energies 8.0–35.2 MeV and charge states from 3+ to 6+ were obtained from the 5-MeV tandem Van de Graaff accelerator at the Institute of Physics of Erlangen-Nürnberg University. Accelerated ion beams were focused by the system of two quadrupole lenses and, after selecting given charge state in the analyzing magnet, were directed onto studied targets. The ion beams collimated to a 2-mm diameter, having intensities 0.5–60 nA, excited the M x rays in thin metallic layers of $_{79}$Au, $_{83}$Bi, $_{90}$Th, and $_{92}$U having thickness between 10 and 30 μg/cm^2, evaporated onto $\sim$20 μg/cm^2 carbon backings. The targets were mounted at an angle 30° with respect to the beam direction. The M x rays excited in the targets were detected by a 30-mm^2 Canberra ultra-low-energy germanium (ULEGe) x-ray detector having a 25-μm beryllium window. The ULEGe detector, which was mounted outside the vacuum chamber perpendicularly to the ion beam direction, had x-ray energy resolution of 150 eV for 6.4 keV. A number of oxygen ions impinging on the target was monitored by surface barrier Si detector recording the elastically backscattered projectiles at an angle 150° with respect to ion beam direction. A typical spectrum of excited M and L x rays, as well as elastically backscattered projectiles, is shown in Fig. 1 for 20.8 MeV O^{4+} ion impact on gold target.

The efficiency of a ULEGe x-ray detector was measured by two complementary methods covering the energy range 1.5–60 keV, following the procedure described in detail in Ref. [10]. We emphasize here that the measurements of detector efficiency in a wide energy range are very crucial for accurate (5%) modeling [10] of the low-energy part (1.5–5 keV) of efficiency curve covering the range of energies of the studied M x rays. First, the calibrated ($\pm$1.8%) x-ray sources of ^{57}Co, ^{133}Ba, ^{152}Eu, and ^{241}Am were used to determine the efficiency for x-ray energies above 12 keV. The x-ray detector efficiency in the photon energy range between 1.5 and 11 keV was measured by bombarding thin targets of low-Z and mid-Z elements with 3-MeV $^1_1$H ions. From the

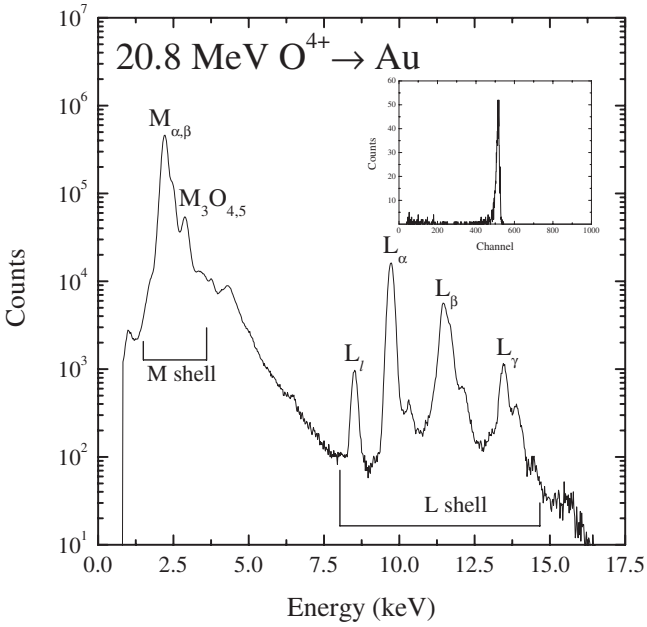

FIG. 1. The measured x-ray spectrum of *M* and *L* x rays of gold excited by 20.8-MeV oxygen ions. The inset shows the spectrum of elastically scattered ions measured at an angle 150° for the normalization of x-ray intensities.

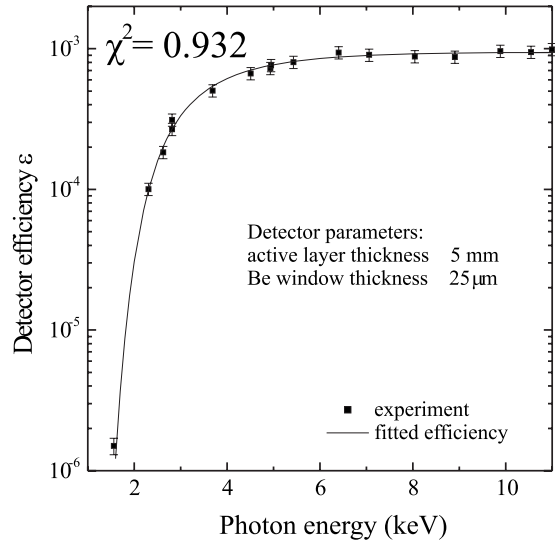

FIG. 2. The measured and fitted efficiency of a semiconductor ULEGe x-ray detector used in the present study. The fitted curve was obtained using a model of detector efficiency described in Ref. [10].

measured *K* x-ray yields, normalized to a number of elastically backscattered ions, the efficiency of a ULEGe detector was determined using the "reference" *K*-shell ionization cross sections (see Ref. [32]) and the screened elastic cross sections [33]. By using this method we were able to determine the efficiency of a ULEGe detector in the energy range 1.5–5 keV with total experimental uncertainties ~4%. The measured and fitted efficiency of a ULEGe detector used in the present study is shown in Fig. 2. Due to strong multiple ionization effects observed in the measured spectra a precise x-ray energy calibration of the detector was needed. In the present experiment the energy calibration was monitored during the measurements by using the radioactive x-ray sources. This approach allowed us to estimate the absolute x-ray energies with the uncertainties better than ±5 eV.

III. MULTIPLE IONIZATION EFFECTS IN X-RAY SPECTRA

The *M* x rays excited in collisions of energetic heavy ions with atoms, when measured by a semiconductor detector, appear to be shifted and broadened [34]. The observed x-ray line shifting and broadening is caused by a presence of the multiple spectator vacancies present during the x-ray emission, which reduce a screening of the nuclear charge. Consequently, the observed x-ray energies are changed toward higher energies with respect to the diagram x-ray lines corresponding to a single vacancy configuration. Additionally, the complex satellite structure of x-ray transitions reflecting a distribution of spectator vacancies in multiply ionized atom during the x-ray emission leads to effective broadening of x-ray lines measured with a semiconductor detector.

In a simple approach based on the independent electron model, which assumes constant ionization probability per electron and constant energy shift per vacancy in a given shell, a binomial distribution of number of vacancies $P_{N_i}(k_i)$ is expected, namely,

$$P_{N_i}(k_i) = \binom{N_i}{k_i} p_i^{k_i}(1-p_i)^{N_i-k_i}, \tag{1}$$

where N_i is a number of electrons, k_i is a number of vacancies, and p_i is the ionization probability per electron in a given shell. In general, the ionization probability per electron appearing in Eq. (1) depends on the impact parameter b, namely, $p_i=p_i(b)$. For direct Coulomb ionization process dominating in asymmetric collisions the ionization probabilities weakly depend on the impact parameter and consequently they can be well approximated (see Ref. [27]) by the ionization probabilities for the zero impact parameter $p_i(0)$, which can be both extracted from the measured x-ray spectra as well as calculated from the SCA approach. Consequently, in discussion of the multiple ionization effects the ionization probabilities per electron for the zero impact parameter $p_i = p_i(0)$ will be considered in this paper.

Within the developed model, which was discussed in detail in Ref. [34], the profile of measured x-ray line modified by the multiple ionization effects can be represented by Gaussian profile having the shifted energy $\langle E\rangle$ and variance $\sigma^2(E)$ expressed, respectively, in terms of average number of vacancies $\langle k_i\rangle = N_i p_i$ and its variance $\sigma^2(k_i) = N_i p_i(1-p_i)$ and calculated average x-ray energy shifts per vacancy δE_i as follows:

$$\langle E\rangle = E_d + \sum_i N_i p_i \delta E_i \tag{2}$$

and, correspondingly,

TABLE I. The calculated Dirac-Fock energy shifts (in eV) for selected M x-ray transitions for gold (Au) and uranium (U).

	Au		U	
Transition	M shell	N shell	M shell	N shell
$M_{4,5}N_{2,3}$	35.6	4.7	47.9	8.8
M_3N_1	28.5	3.8	35.5	8.9
$M_5N_{6,7}$	38.3	6.2	49.1	8.2
M_4N_6	36.8	3.9	50.5	8.2
M_3N_5	31.4	7.6	39.7	9.2
M_2N_1	32.0	3.7	42.8	8.4
M_3O_1	40.5	13.3	58.4	20.3
$M_3O_{4,5}$	46.8	15.4	63.1	24.5
M_2N_4	34.1	5.2	45.7	9.6
M_2O_4	48.0	13.0	70.2	25.0
$M_1O_{2,3}$	45.8	14.3	62.1	21.9

$$\sigma^2(E) = \sum_i N_i p_i (1 - p_i)\,\delta E_i^2 + \sigma_G^2, \tag{3}$$

where E_d is the energy of a diagram line and σ_G represents the variance of internal x-ray energy spread in a detector. For illustration, the M- and N-shell ionization probabilities per electron $p_i(0)$ measured for oxygen ion impact on the studied elements are below 0.05 and 0.25 [35], respectively, corresponding to the mean number of vacancies less than 1 and 8 in the M and N shells.

This model, called the averaged binomial model (ABM), allows us to analyze the M-shell x-ray spectra modified by the multiple ionization effects, which will be discussed in Sec. IV. In order to apply this approach one has to know the values of x-ray energy shifts per vacancy, δE_i, entering Eqs. (2) and (3). The Dirac-Fock calculations of x-ray energy shifts were performed for selected M-N,O transitions for Au and U. For Bi and Th their linearly interpolated values were used, knowing that the energy shifts per vacancy exhibit nearly linear dependence on the atomic number [36,37]. The calculated Dirac-Fock values of x-ray energy shifts per vacancy for selected M x-ray transitions in Au and U are summarized in Table I.

IV. ANALYSIS OF *M* X-RAY SPECTRA

The M x rays excited in the studied atoms (Au, Bi, Th, and U) exhibit a complex structure which cannot be fully resolved by a semiconductor x-ray detector (see Fig. 1). A diagram of M x-ray transitions of interest is shown in Fig. 3 together with estimated relative intensities of individual x-ray lines shown for uranium excited by 35.2 MeV oxygen ions. The measured M x-ray spectra are dominated by $M_{\alpha_{1,2}}(M_5N_{6,7})$ and $M_\beta(M_4N_6)$ transitions, while the $M_{\zeta_{2,1}}(M_{4,5}N_{2,3})$, M_3N_1, $M_\gamma(M_3N_5)$, M_2N_1, M_3O_1, $M_3O_{4,5}$, M_2N_4, M_2O_4, and $M_1O_{2,3}$ transitions are weaker, but strong enough to be observed and thus included in M x-ray spectra analysis.

The interpretation of complex M x-ray spectra excited by oxygen ion is a difficult task taking into account that the energy spacing of individual x-ray lines is of the order of energy resolution of a semiconductor x-ray detector. Moreover, the multiple ionization effects shifting and broadening the x-ray lines, by tens of electron volts (see Table I), make practically inapplicable a standard method of x-ray spectra analysis by fitting individual Gaussian x-ray lines with the energies being completely free fitting parameters. For this reason, in the present paper, we propose a different approach of analysis of complex M x-ray spectra, which is based on a description of the multiple ionization effects given in Sec. III [see Eqs. (2) and (3)]. Using this approach, in the first stage, the ionization probabilities per electron for the zero impact parameter $p_i(0)$ for the M and N shells are derived from the measured L x rays following the method described earlier (see Ref. [38]). This can be done quite accurately for the L x rays since characteristic impact parameter for the ionization of the L shell is much smaller than the corresponding one for the M and N shells. The measured ionization probabilities $p_i(0)$ for the M and N shells for oxygen ion impact, which were used in the present study, are compared with the predictions of the SCA calculations in Fig. 4. These results were discussed in detail in Ref. [35]. In the next step of M x-ray spectra analysis the ionization probabilities for the M and N shells derived from the measured L x rays and the Dirac-Fock x-ray energy shifts from Table I were used to calculate

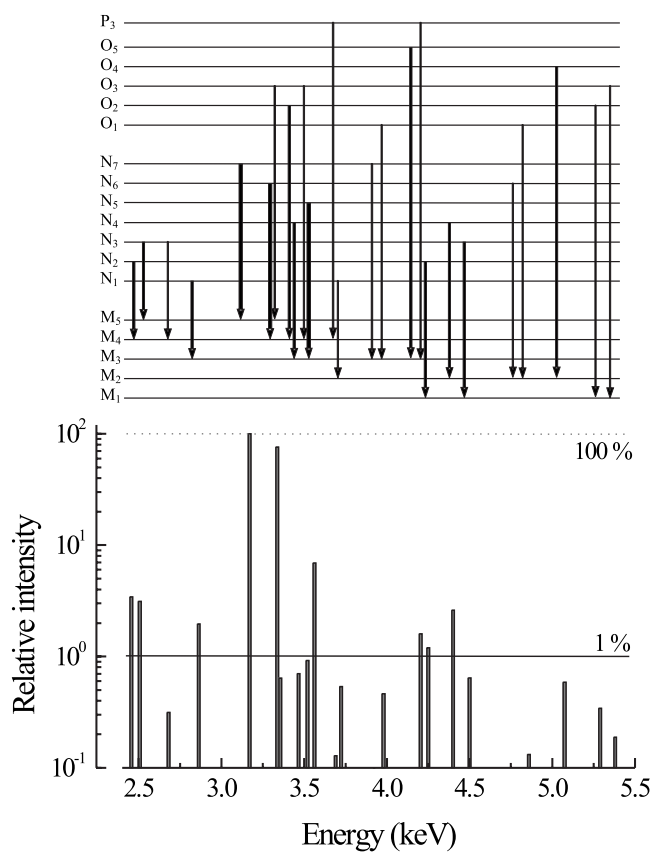

FIG. 3. A scheme of energy levels in M, N, and O shells showing the diagram M x-ray transitions with their relative intensities calculated for uranium excited by 35.2 MeV oxygen ions.

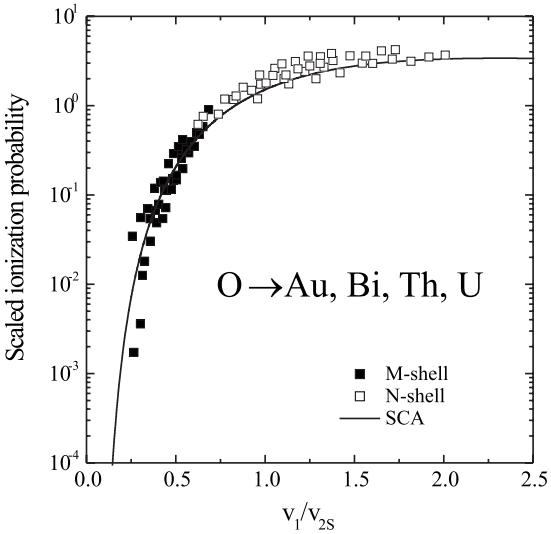

FIG. 4. Scaled ionization probabilities for zero impact parameter $p_i(0)/(Z_1/v_1 n_i)^2$ for the M and N shells, n_i=3 and 4, respectively, measured for oxygen ion impact on studied elements (from Ref. [35]) plotted versus the relative projectile velocity in comparison with the predictions of the SCA calculations.

the expected positions and widths [Eqs. (2) and (3)] of M x-rays lines shifted and broadened by the multiple ionization effects. Finally, by knowing approximately, but reasonably well, the starting values of energies and widths the M x-ray lines were fitted by the least-squares method allowing only for very fine adjustment of energies and widths, in the range of 10–15%. This approach was found to be sensitive enough for resolving uniquely a structure of measured M x rays. We note here that the crucial points for applying the proposed approach are the following: (i) independent determination of the ionization probabilities from the L x rays measured simultaneously with studied M x rays, (ii) realistic modeling of the multiple ionization effects [Eqs. (2) and (3)] and, finally, (iii) application of restricted fitting of energies and widths.

An example of such analysis of measured M x-ray spectrum of uranium excited by 11.2-MeV oxygen ions is shown in Fig. 5. In order to verify the correctness and accuracy of applied fitting procedure the measured and fitted spectra for uranium were compared with the simulated spectrum of M x-ray satellites based on the binomial model of vacancies distribution described in Sec. III. The positions and widths of simulated satellites were given by Eqs. (2) and (3) with the M- and N-shell ionization probabilities derived from measured L x rays. The intensities and background shape in the simulated spectrum were taken from the measured spectrum. The measured, fitted, and simulated spectra of uranium M x rays, which are compared in Fig. 6, clearly demonstrate a correctness of the present method of M x-ray spectra analysis. This fitting approach was found to be sensitive on fine details of the measured spectra. For instance, the widths of fitted M x-ray lines were found to be systematically slightly wider by about 5–15 eV than ones calculated from Eq. (3). This observation can be explained by the fact that the individual x-ray satellites are not single, equally spaced, x-ray

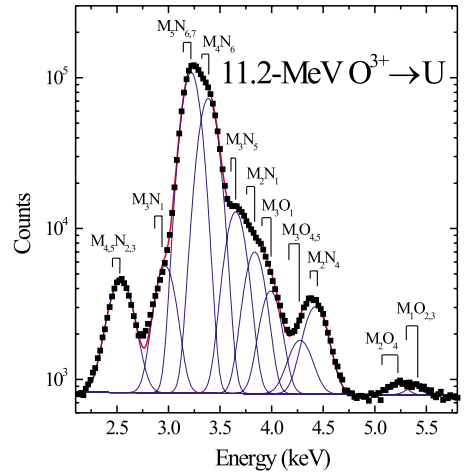

FIG. 5. (Color online) Measured M x-ray spectrum of uranium excited by 11.2 MeV oxygen ions showed with the fitted structure of Gaussian profiles for M-shell x-ray transitions.

lines as it was assumed in the binomial model used. In fact, the M x-ray satellites have complex structure (see Ref. [39]) which can be obtained using the relativistic multiconfiguration Dirac-Fock (MCDF) calculations. As an illustration, in Fig. 7 the Gaussian-convoluted spectra of the satellite $M_{\alpha_1}(M^{-1})$ x-ray transition in gold assuming a single transition having shifted energy (ABM model) and the MCDF multiplet structure are compared to demonstrate the discussed widening effect.

V. RESULTS

A. *M* x-ray production cross sections

The intensities of resolved M x-ray transitions were used to determine the M-ray production cross sections for these transitions. The x-ray cross sections were obtained by nor-

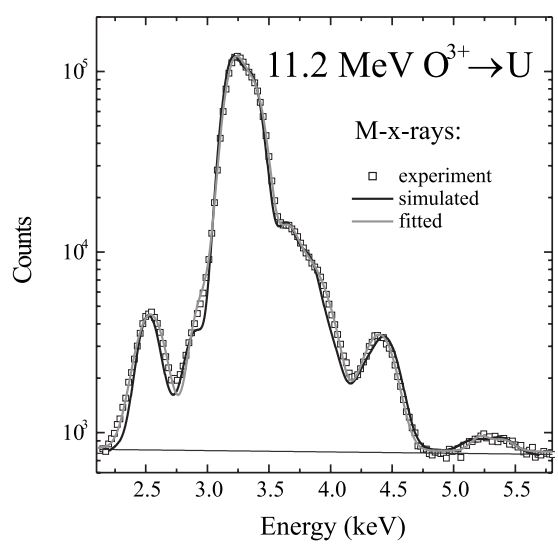

FIG. 6. Comparison of measured M x-ray spectrum for uranium excited by 11.2 MeV oxygen ions with the fitted and simulated spectra (see the text).

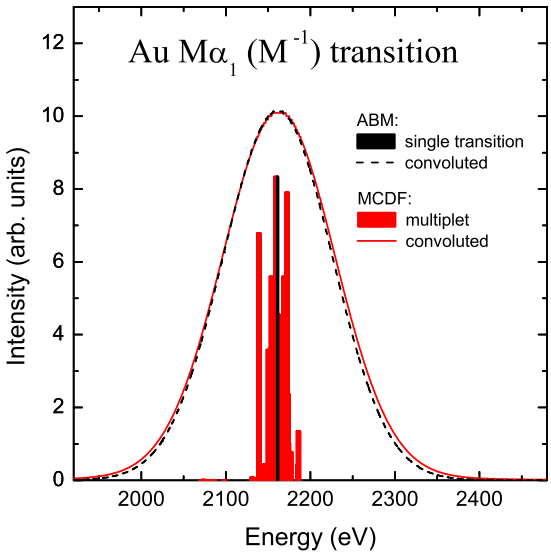

FIG. 7. (Color online) Comparison of Gaussian-convoluted profiles of the satellite $M_{\alpha_1}(M^{-1})$ x-ray transition in gold assuming a single transition according to the simplified ABM model discussed and a multiplet structure obtained from the MCDF calculations which demonstrate the widening effect.

malizing the x-ray yields, corrected for the efficiency of the ULEGe x-ray detector, to a number of elastically scattered oxygen ions which were measured by a silicon surface barrier detector. Additionally, the cross sections were corrected for the effects of projectile energy-loss and x-ray self-absorption in the targets following a procedure described in Ref. [11]. This correction was very small, below 2%. Derived x-ray production cross sections for all resolved M x-ray transitions were summed to obtain the total M x-ray production cross sections, while the cross sections for the $M_5N_{6,7}$, M_4N_6, M_3N_5, M_2N_4, and $M_1O_{2,3}$ x-ray transitions were further used to determine the M-subshell ionization cross sections. The experimental uncertainties of total M x-ray production cross sections were in the range 7–10%, being mostly affected by the uncertainties associated with determination of efficiency of ULEGe detector. The measured values of total M x-ray cross sections are summarized in Table II. In Fig. 8 the measured M x-ray production cross sections for $M_5N_{6,7}$, M_4N_6, M_3N_5, M_2N_4, and $M_1O_{2,3}$ x-ray transitions in gold bombarded by oxygen ions are compared with the predictions of the ECPSSR and SCA calculations. The total M x-ray production cross sections measured for $_{79}$Au, $_{83}$Bi, $_{90}$Th, and $_{92}$U are compared in Figs. 9–12 with the predictions of different theoretical approaches, namely, the ECPSSR, ECUSAR, SCA, PWBA, and BEA, which will be discussed in Sec. VI. For calculation the theoretical M x-ray production cross sections shown in Figs. 8–12, the M-shell fluorescence, and Coster-Kronig yields are needed, which additionally can be affected by the multiple ionization effects. This is an important aspect of the present work which is discussed in details in Sec. V B. We note only here that the calculated *total* M x-ray production cross sections, shown in Figs. 9–12, are generally less sensitive than the *individual* M x-ray cross sections to possible modifications of the M-shell decay rates due to the multiple ionization effects.

TABLE II. The measured total M x-ray production cross sections (in barns) for oxygen impact on Au, Bi, Th, and U. Note: here 1.41+4 means 1.41×10^4 barn.

Energy (MeV)	Element			
	Au	Bi	Th	U
8.0	1.41+4	8.51+3	3.98+3	2.87+3
11.2	2.62+4	2.09+4	9.68+3	7.37+3
14.4	4.05+4	3.32+4	1.62+4	1.20+4
17.6	6.52+4	4.26+4	2.59+4	1.80+4
20.8	7.89+4	5.31+4	3.38+4	2.38+4
22.4	8.60+4	6.22+4	4.17+4	2.83+4
25.6	1.02+5	6.76+4	4.71+4	3.49+4
28.8	1.15+5	7.81+4	5.62+4	4.08+4
32.0	1.27+5	8.84+4	6.01+4	4.49+4
35.2	1.29+5	9.48+4	6.59+4	4.84+4
Uncertainty (%)	9–12	8–12	7–10	7–10

B. *M*-shell decay rates in multiply ionized atoms

In order to relate the M-shell x-ray production and ionization cross sections the M-shell radiative and nonradiative decay rates determining the fluorescence and Coster-Kronig yields are needed. However, the multiple ionization affects the radiative, Coster-Kronig, and Auger rates in various ways, which was discussed in detail in Ref. [40]. In multiply ionized atom the M-shell decay rates can be changed due to the following effects: (i) reduced number of electrons available for given transition, (ii) closing of selected Coster-

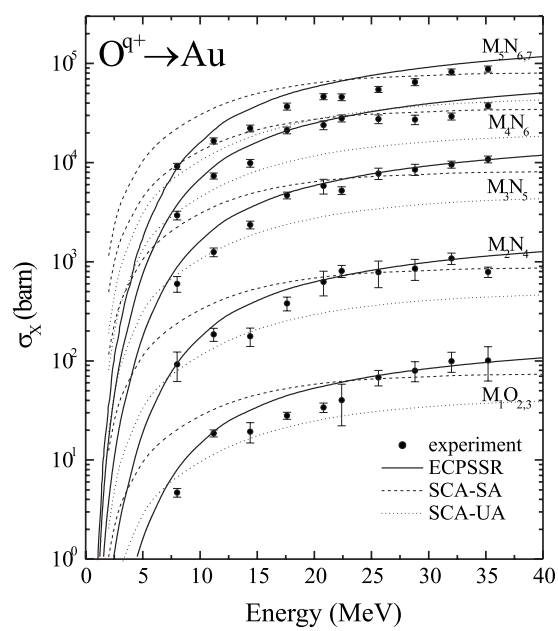

FIG. 8. Measured M x-ray production cross sections for selected transitions for oxygen ion impact on gold. The experimental results are compared with the theoretical predictions calculated according to the ECPSSR and SCA approaches discussed in Sec. VI.

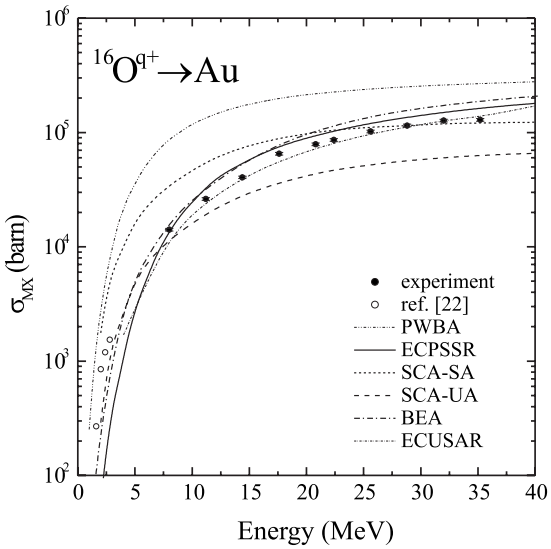

FIG. 9. The measured *M* x-ray production cross sections for oxygen impact on gold. The experimental results are compared with the predictions of the PWBA, ECPSSR, ECUSAR, SCA, and BEA calculations which are discussed in Sec. VI. The results from our previous low-energy experiment [22] are shown for comparison.

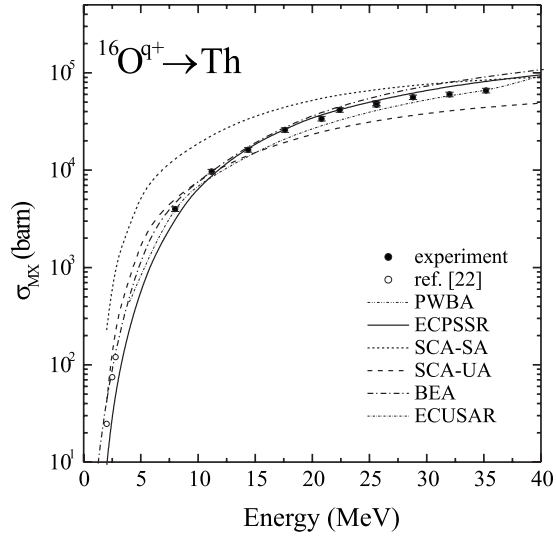

FIG. 11. The measured *M* x-ray production cross sections for oxygen impact on thorium. The experimental results are compared with the predictions of the PWBA, ECPSSR, ECUSAR, SCA, and BEA calculations which are discussed in Sec. VI. The results from our previous experiment [22] are shown for comparison.

Kronig transitions which become energetically forbidden, and (iii) modification of electronic wave function. The first two effects can be treated within simplified models in terms of the ionization probabilities for the *M* and *N* shells, while the wave function effect is much more difficult to be accounted for due to complex atomic structure calculations needed for various multivacancy configurations. Consequently, this effect was neglected here, which was justified by a rather small number of vacancies created in the *M* shell by the multiple ionization. The simplest effect of reduction of a number of electrons available in multiply ionized atom for a given transition can be accounted for by the statistical scaling [41] of single vacancy decay rates by a fraction of available electrons.

The change in electron binding energies in the multiply ionized atoms can also have a strong effect on the Coster-Kronig transitions, in particular, for those for which the Coster-Kronig electrons have low energies, being of the order of energy shift of the electron binding energy. Such Coster-Kronig transitions can be energetically forbidden (closed) in multiply ionized atoms. This happens when the kinetic energy of Coster-Kronig electron becomes negative, which can be estimated by using a simple model of electron

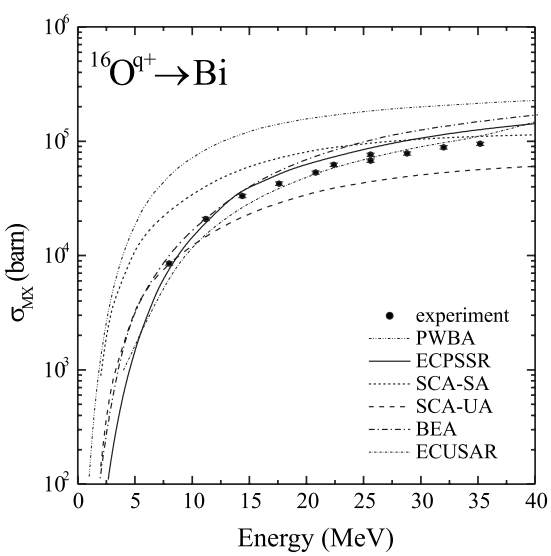

FIG. 10. The measured *M* x-ray production cross sections for oxygen impact on bismuth. The experimental results are compared with the predictions of the PWBA, ECPSSR, ECUSAR, SCA, and BEA calculations which are discussed in Sec. VI.

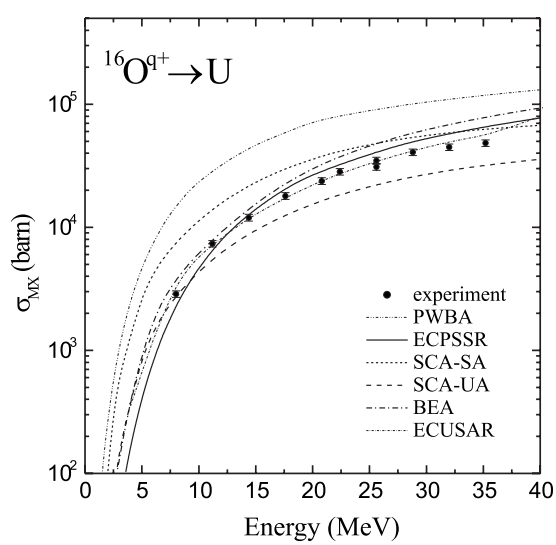

FIG. 12. The measured *M* x-ray production cross sections for oxygen impact on uranium. The experimental results are compared with the predictions of the PWBA, ECPSSR, ECUSAR, SCA, and BEA calculations which are discussed in Sec. VI.

binding based on the so-called "$Z+1$" rule [42]. Using this approach we have calculated that the closing effect can occur for the $M_1-M_2N_{6,7}$, $M_2-M_3N_{4,5}$, and $M_3-M_5N_{6,7}$ Coster-Kronig transitions in studied atoms multiply ionized by oxygen ions. Closing of these transitions, contributing substantially to the M-shell Coster-Kronig and total decay rates, had strong effect on the fluorescence and Coster-Kronig yields for the M shell. For illustration, the modified M-shell fluorescence and Coster-Kronig yields calculated for gold multiply ionized by oxygen ions are shown in Figs. 13 and 14. Consequently, the effects of modification of M-shell fluorescence and Coster-Kronig yields were found to be important for deriving the M-subshell ionization cross sections from the measured x-ray production cross sections, which will be discussed in Sec. V C.

C. *M*-subshell ionization cross sections

In order to describe the emission of M x rays from an ionized atom one has to take into account the M-subshell ionization cross sections, the Coster-Kronig transitions leading to the rearrangement of vacancies prior to x-ray emission and, finally, a probability for radiative decay of a vacancy by emission of a given M x-ray transition. For the M shell, an ionized atom with a single vacancy in one of the M subshells decays radiatively with emission of x-ray photon, or nonradiatively, by emitting of an electron via the Auger, Coster-Kronig, or super-Coster-Kronig process. In order to relate the M_i-subshell ionization cross sections, σ_{M_i}, with the x-ray production cross section $\sigma_{M_iX_k}$ for a given M x-ray transition (M_iX_k), filling an initial vacancy in the M_i subshells, first, the vacancy *rearrangement* processes taking place prior to a moment of x-ray emission have to be taken into account. More precisely, a vacancy created at a moment of collision in the M_i subshell can be transferred to higher M_j subshell ($j>i$) via the Coster-Kronig or super-Coster-Kronig processes with a probability which is given by the corresponding (super-) Coster-Kronig yield f_{ij} [43]. Consequently, to account for the vacancy rearrangement enhancing a number of vacancies in the subshell due to the (super-) Coster-Kronig transitions, the effective Coster-Kronig yield $\bar{f}_{ij}$ are introduced here, which are the probabilities for transferring a vacancy between the M_i and M_j subshells taking into account all possible paths (see also Refs. [1,43]). Consequently, the *effective* Coster-Kronig yields $\bar{f}_{ij}$ can be expressed in terms of Coster-Kronig yields f_{ij} as follows:

$$\bar{f}_{ij}=f_{ij}+\sum_{i<k<j} f_{ik}f_{kj}+\sum_{i<k<k'<j} f_{ik}f_{kk'}f_{k'j} + \sum_{i<k<k'<k''<j} f_{ik}f_{kk'}f_{k'k''}f_{k''j} \tag{4}$$

with additional condition $\bar{f}_{ii}=1$. Introducing the M-subshell fluorescence yields ω_i and relative emission rates $\Gamma_{X_k}(i)/\Gamma_X(i)$ for individual M x-ray transitions, the M-shell x-ray production cross section $\sigma_{M_iX_k}$ can be expressed as follows:

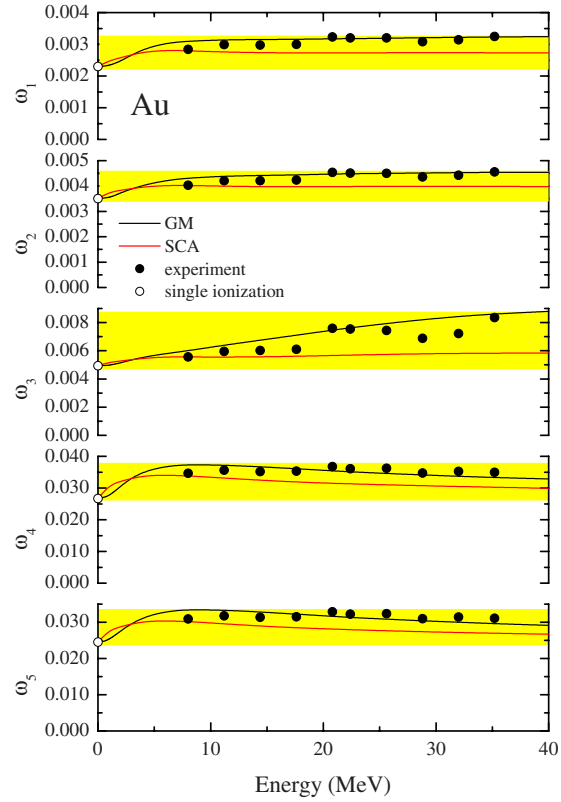

FIG. 13. (Color online) Fluorescence yields for gold changed by multiply ionization in comparison of the theoretical predictions of SCA and GM models.

$$\sigma_{M_iX_k}=[\Gamma_{X_k}(i)/\Gamma_X(i)]\cdot\omega_i\sum_{j\le i}\bar{f}_{ji}\sigma_{M_j}. \tag{5}$$

Using this notation the *total* M-shell x-ray production cross section, discussed in the previous sections, reads as follows:

$$\sigma_{MX}=\sum_{i=1}^{5}\omega_i\sum_{j\le i}\bar{f}_{ji}\sigma_{M_j}. \tag{6}$$

However, the total M x-ray production and ionization cross sections can be directly related by introducing the effective M-shell fluorescence yield $\bar{\omega}_M$, namely,

$$\sigma_{MX}=\bar{\omega}_M\sigma_M. \tag{7}$$

It is important to note that the effective M-shell fluorescence yield $\bar{\omega}_M$ can be well approximated, usually within 1% by simply approximate expression [11]

$$\bar{\omega}_M\approx 0.4(\omega_4+f_{45}\omega_5)+0.6\omega_5. \tag{8}$$

This approximation, in fact, reflects a dominating role of the $M_{4,5}$ subshells, weighted by corresponding statistical factors, in M-shell ionization. In the present paper Eqs. (7) and (8) were used to calculate the total M x-ray production cross sections for the BEA model, for which only the total M-shell ionization cross sections can be calculated.

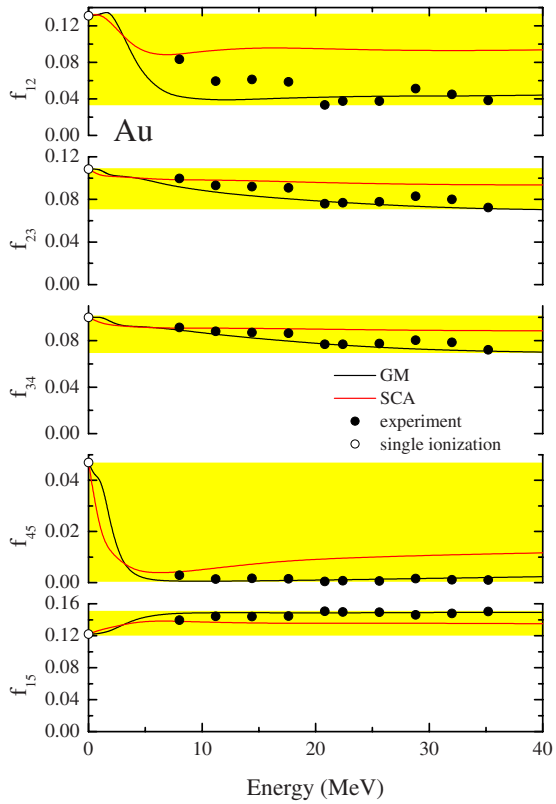

FIG. 14. (Color online) Selected Coster-Kronig yields for gold changed by multiply ionization in comparison of the theoretical predictions of SCA and GM models.

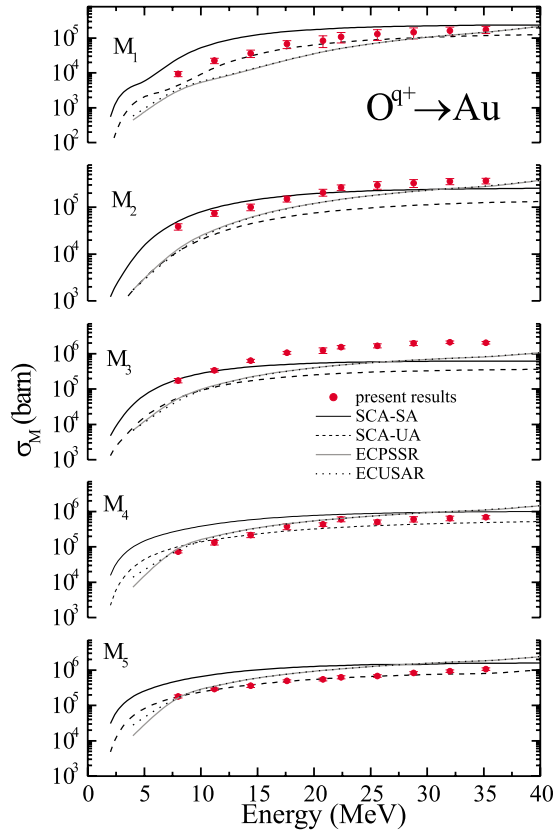

FIG. 15. (Color online) *M*-subshell ionization cross sections for oxygen impact on gold. Experimental results are compared with the predictions of the ECPSSR, ECUSAR, and SCA calculations which are discussed in Sec. VI.

The *M*-shell fluorescence and Coster-Kronig yields appearing in Eqs. (5) and (6) are expressed in terms of the *M*-shell decay rates, namely, $\omega_i=\Gamma_X(i)/\Gamma(i)$ and $f_{ij}=\Gamma_{CK}(ij)/\Gamma(i)$ with $\Gamma(i)=\Gamma_X(i)+\Gamma_{CK}(i)+\Gamma_A(i)$ being the total *M*-shell decay rate, i.e., a sum of rates for radiative (X), Coster-Kronig (CK), and Auger (A) processes. In multiply ionized atoms, as it was discussed above, the decay rates are modified, which can be described in terms of the measured ionization probabilities for the *M* and *N* shells. It is important to emphasize here that such modified *M*-shell decay rates were used in the present study in calculation of the theoretical *M* x-ray production cross sections as well as derivation of the experimental *M*-subshell ionization cross sections [see Eqs. (5) and (6)]. In particular, the x-ray production cross sections for $M_{\alpha_{1,2}}(M_5N_{6,7})$, $M_\beta(M_4N_6)$, $M_\gamma(M_3N_5)$, M_2N_4, and $M_1O_{2,3}$ x-ray transitions in gold bombarded by oxygen ions, which were calculated using the discussed theories describing the *M*-subshell ionization, are shown in Fig. 8, while the calculated total *M* x-ray production cross sections for $_{79}$Au, $_{83}$Bi, $_{90}$Th, and $_{92}$U atoms are compared with the data in Figs. 9–12.

A reliable resolution of a structure of *M* x rays excited by oxygen ions allowed a determination of experimental *M*-subshell ionization cross sections σ_{M_i} from the measured x-ray production cross sections for the $M_{\alpha_{1,2}}(M_5N_{6,7})$, $M_\beta(M_4N_6)$, $M_\gamma(M_3N_5)$, M_2N_4, and $M_1O_{2,3}$ x-ray transitions. This was achieved by solving a system of linear equations [see Eq. (5)] relating the corresponding cross sections. The measured *M*-subshell ionization cross sections for oxygen impact on $_{79}$Au, $_{83}$Bi, $_{90}$Th, and $_{92}$U are compared with theoretical predictions in Figs. 15–18. Since the *M*-shell ionization cross sections are expected to be approximately universal, when expressed in terms of the scaling parameter ξ_i (see Sec. VI), the reduced *M*-shell ionization cross sections measured for all studied elements are compared with discussed theoretical predictions in Fig. 19.

VI. THEORIES OF *M*-SHELL IONIZATION

In asymmetric collisions ($Z_1 \ll Z_2$) discussed in the present paper the *M*-shell vacancies are created mainly by direct Coulomb ionization. Other competing processes, namely, the electron capture (EC) to the projectile [44–47], the molecular excitation [48–54], and the recoil ionization [55–58] are negligible in comparison with direct Coulomb ionization. The available theoretical approaches treating the direct ionization were formulated using the PWBA, the SCA, and the BEA.

A. PWBA

A nonrelativistic treatment of direct Coulomb ionization using the plane-wave Born approximation was introduced by Bethe [59], while the application of the PWBA approach to

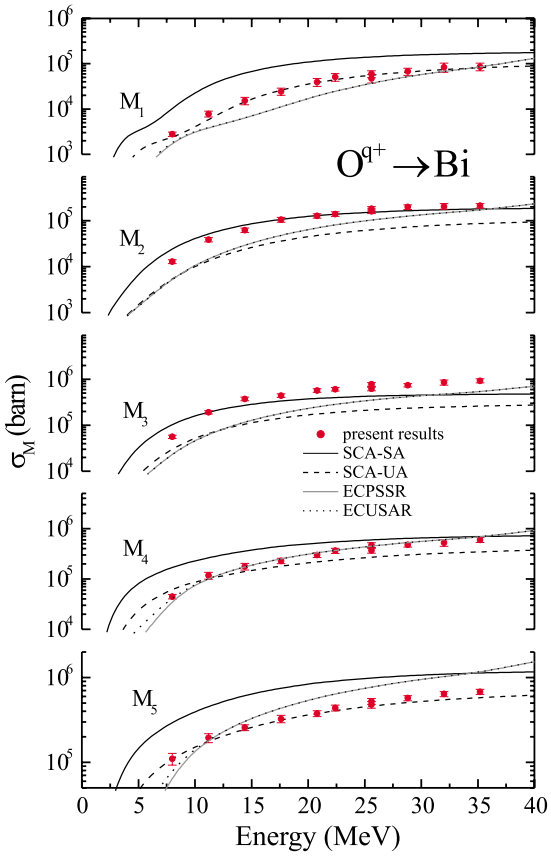

FIG. 16. (Color online) M-subshell ionization cross sections for oxygen impact on bismuth. Experimental results are compared with the predictions of the ECPSSR, ECUSAR, and SCA calculations which are discussed in Sec. VI.

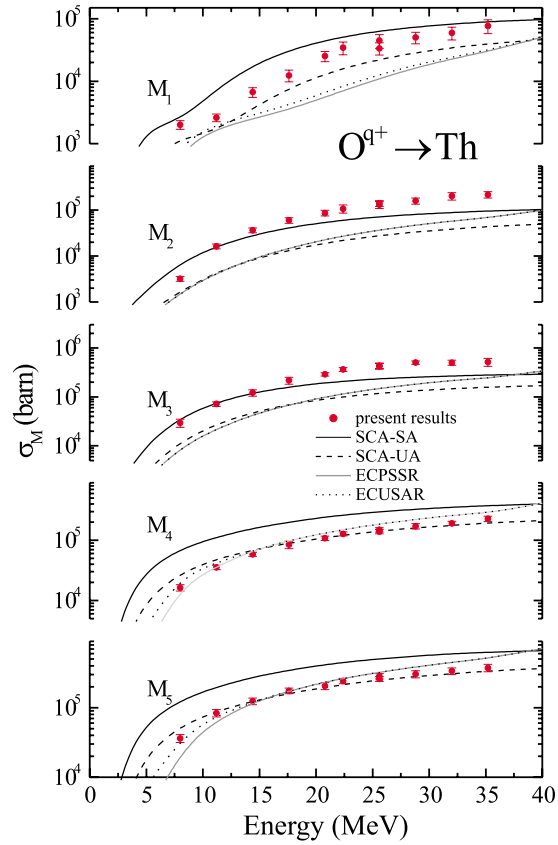

FIG. 17. (Color online) M-subshell ionization cross sections for oxygen impact on thorium. Experimental results are compared with the predictions of the ECPSSR, ECUSAR, and SCA calculations which are discussed in Sec. VI.

the M-shell ionization by heavy, charged particles was systematically presented in Refs. [26,60]. An applicability of the PWBA approach to treat direct Coulomb ionization is generally well justified for asymmetric ($Z_1 \ll Z_2$) collisions due to a weak perturbation of the initial electronic state by the projectile.

The PWBA approach was further developed [30,61] to include the effects which go beyond the first-order treatment, namely the binding, polarization, Coulomb deflection, energy-loss and relativistic effects, which is known as the ECPSSR theory [30,61]. The predictions of the PWBA and the ECPSSR theory can be expressed by a dynamical scaling parameter ξ_i which is proportional to a ratio of the projectile v_1 and classical M-shell electron velocity $v_{M_i}=(2E_{M_i}/m_e)^{1/2}$,

$$\xi_i = (2/\sqrt{\theta_i})v_1/v_{M_i}. \tag{9}$$

The scaled electron binding energy $\theta_i=n^2E_{M_i}/Z_{M_i}^2\mathcal{R}$ describing the outer screening is expressed by the electron binding energy E_{M_i} and the screened target atomic number Z_{M_i}, with n being the principal quantum number and $\mathcal{R}$ the Rydberg constant. Using the scaling parameters ξ_i and θ_i the nonrelativistic PWBA ionization cross sections for the M-shell reads [60]

$$\sigma_{M_i}^{\mathrm{PWBA}}(\xi_i,\theta_i) = 8\pi a_0^2(Z_1^2/Z_{M_i}^4)F_{M_i}(\xi_i,\theta_i)/\theta_i, \tag{10}$$

where the $F_{M_i}(\xi_i,\theta_i)$ functions were tabulated in Ref. [60] and a_0 denotes the Bohr radius. For the M shell the θ_i parameter has nearly constant value and, additionally, for low energies ($\xi_i \ll 1$) the PWBA scaling function $F_{M_i}(\xi_i,\theta_i) \approx F_{M_i}(\xi_i)$. This observation shows that the M-shell ionization cross sections are expected to be universal with respect to ξ_i in the low-energy limit [60,62].

In the ECPSSR theory the ionization cross sections for M_i subshell, $\sigma_{M_i}^{\mathrm{ECPSSR}}$, are expressed in terms of the PWBA cross section, $\sigma_{M_i}^{\mathrm{PWBA}}(\xi_i,\theta_i)$, with the modified scaling parameters $\xi_i \rightarrow \xi_i/\zeta_i$ and $\theta_i \rightarrow \zeta_i\theta_i$, where ζ_i is dimensionless parameter describing a change in the electron binding energy, times the Coulomb deflection factor $C_i(x_i)$ and the energy-loss factor $f_i(z_i)$, namely (see [30,61])

$$\sigma_{M_i}^{\mathrm{ECPSSR}} = C_i(x_i)f_i(z_i)\sigma_{M_i}^{\mathrm{PWBA}}(\xi_i^R/\zeta_i,\zeta_i\theta_i). \tag{11}$$

The exact forms of ξ_i^R, ζ_i, x_i, and z_i quantities can be found in Refs. [30,61]. The parameter $\zeta_i(Z_1,\xi_i)$, which describes in the ECPSSR theory the binding effect, i.e., an increase in the electron binding energy due to a presence of a projectile in the vicinity of target atom nucleus, for the *extreme adiabatic* regime $\xi_i \simeq 0$ tends to $\zeta_i(\xi_i=0)=1+2Z_1/\theta_i Z_{M_i}$ [61]. This value is higher than the

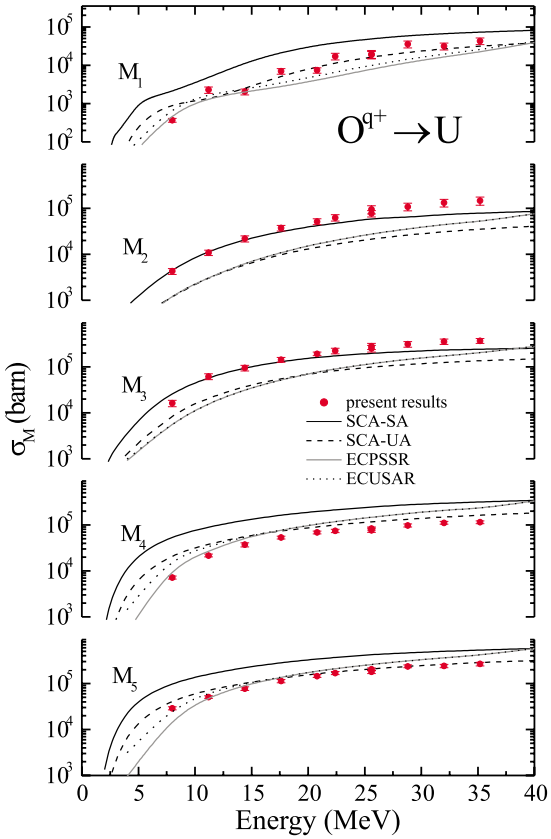

FIG. 18. (Color online) *M*-subshell ionization cross sections for oxygen impact on uranium. Experimental results are compared with the predictions of the ECPSSR, ECUSAR, and SCA calculations which are discussed in Sec. VI.

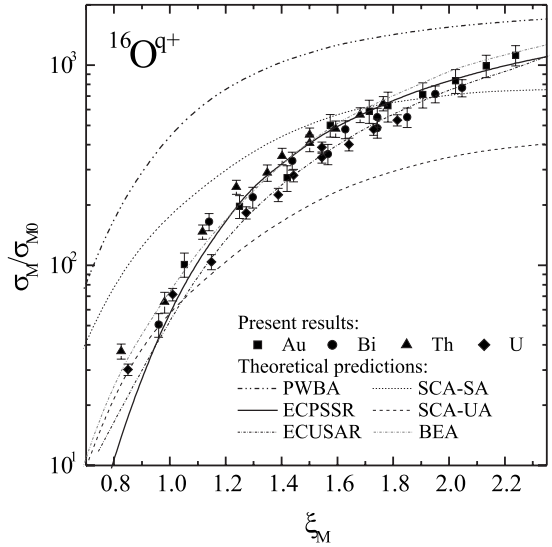

FIG. 19. The total *M*-shell ionization cross sections for oxygen ions in the energy range of 8.0–35.2 MeV plotted as the reduced ionization cross section σ_M/σ_{M0} versus the scaled velocity parameter ξ_M for all targets. The experimental results are compared with the predictions of the PWBA, ECPSSR, ECUSAR, SCA, and BEA calculations which are discussed in Sec. VI.

physically expected ratio of electron binding energies in the united atom, $E_{M_i}(Z_1+Z_2)$, and separated atom, $E_{M_i}(Z_2)$, limits, namely, $E_{M_i}(Z_1+Z_2)/E_{M_i}(Z_2) \simeq (1+Z_1/Z_{M_i})^2$. An overestimation of the electron binding effect in adiabatic regime, quantified by $\zeta_i(\xi_i=0)$, accounts for the observed systematic underestimation of the ECPSSR *M*-shell ionization cross sections at very low energies. This can be explained by a strong dependence of *M*-shell ionization cross sections on ζ_i, namely, $\sigma_{M_i}^{\mathrm{ECPSSR}} \propto 1/\zeta_i^{13}$ for dominating $M_{4,5}$ subshells for low energies [60].

For this reason the ECPSSR theory has been recently modified [31] to correct for the observed overestimation of the binding effect. In this approach, called the ECUSAR theory [31], a saturation of the corrected electron binding energy at its UA limit value was proposed. Consequently, both the united and separated atom electron binding energies are reproduced in the ECUSAR theory. We note that for asymmetric collisions the predictions of *M*-shell ionization according to the ECPSSR and ECUSAR theories agree quite well, within 3%, over wide energy range, with exception of the lowest energies below 1 MeV/amu for which the predictions of both theories become systematically different.

B. SCA

The cross section of inner-shell ionization by charged particles can be calculated in the semiclassical approximation which was used by Bang and Hansteen [27] for description of the ionization process. In this approach a charged particle is moving along the classical trajectory $\mathbf{R}(b,t)$, which for a given impact parameter b is parametrized by time t, while the ionization is described quantum mechanically. A validity of the SCA approach is given by the Bohr criterion for the classical trajectory [63],

$$\frac{2Z_1Z_2e^2}{\hbar v_1} \gg 1, \tag{12}$$

implying that the SCA approach is expected to be valid in the low-energy regime.

The SCA amplitude for the excitation of initially bound electron in a state $|\varphi_i\rangle$ to the final state $|E_f\rangle$ in the continuum can be expressed using the first-order time-dependent perturbation theory as follows:

$$a_{if}(b,E_f) = -\frac{i}{\hbar}\int_{-\infty}^{+\infty} dt\, e^{(i/\hbar)(E_f-E_i)t}\langle E_f|\frac{-Z_1e^2}{|\mathbf{r}-\mathbf{R}(b,t)|}|\varphi_i\rangle. \tag{13}$$

in the SCA approach is expressed by the following formula:

$$\sigma_{M_i}^{\mathrm{SCA}} = 2\pi\int_0^{\infty} db\, b\left(\sum_{E_f}|a_{if}(b,E_f)|^2\right), \tag{14}$$

where the summation extends over possible electron final states $|E_f\rangle$ in the continuum. The SCA ionization cross sections for the straight-line trajectory and nonrelativistic hydrogenic wave functions for the *M* shell were tabulated by Hansteen *et al.*[64] (see also Refs. [65–67]). However, for a more realistic description of the ionization process within the SCA the hyperbolic projectile trajectories and relativistic

wave functions were used in more complex numerical SCA calculations (see, e.g., Refs. [58,67,68]).

For interpretation of the measured M-shell ionization cross sections the SCA calculations were performed following basic Eqs. (13) and (14). In these calculations, which are described in detail in Ref. [58], the hyperbolic projectile trajectories and hydrogenic relativistic electronic wave functions were used. The binding effect, caused by an increased electron binding energy due to a presence of the projectile in the vicinity of the target nucleus, was included in the SCA calculations in two extreme cases, namely the separated (SCA-SA) and united (SCA-UA) atom limits. Noting that a characteristic impact parameter for the ionization, the so-called adiabatic radius $r_{\mathrm{ad}}=\hbar v_1/E_{M_i}$, scales with the projectile velocity one expects that the SCA-UA approximation is valid for the low energies, while for the high energies the SCA-SA treatment is adequate.

C. BEA

A formulation of the binary-encounter approximation, which goes back to classical description of ionization process, was developed almost a century ago by Thomson [69]. In this treatment the ionization by ion impact is treated as a two-body collision in which the energy transfer to the electron exceeds its binding energy and the velocity distribution of electron is given by the electronic wave function in the momentum space. This approach to the atomic collisions has been used to formulate the BEA [70–73], which was further developed to treat the inner-shell ionization by heavy particles [28,29,74]. The BEA model predicts a universal scaling of total ionization cross sections for arbitrary shell which are expressed in terms of the relative projectile velocity $V=v_1/v_{M_i}$ as follows [29]:

$$\sigma_{M_i}^{\mathrm{BEA}} = (N_i Z_1^2 \sigma_0 / E_{M_i}) G_i(V), \tag{15}$$

where N_i is a number of electrons in given shell and a constant σ_0 can be found in Ref. [29]. The scaling function $G_i(V)$ was tabulated for different $n\ell$ states with $n \leq 2$ in Ref. [29]. For higher shells, by using the arguments of Fock theorem [75] stating that a velocity distribution of electrons in a closed shell is the same as for the s state, the total BEA ionization cross sections for arbitrary closed shell can be obtained using the scaling function for the K shell. For this reason only the total M-shell ionization cross sections calculated in the BEA model were discussed here (see Figs. 9–12). Due to this limitation, and noting additionally that the classical BEA model is less rigorous than quantal PWBA and SCA based treatments, the present M-shell ionization data will be compared in more detail with the SCA, ECPSSR, and ECUSAR approaches.

VII. DISCUSSION

The M-shell x-ray production cross sections measured in the present work for heavy ($_{79}$Au, $_{83}$Bi, $_{90}$Th, and $_{92}$U) atoms in collisions with oxygen ions in the energy range 8.0–35.2 MeV were obtained by applying a developed approach for the M x-ray spectra analysis and interpretation of the data which takes into account the multiple ionization effects playing an important role for heavy ion impact. In this approach, the intensities, energies, and widths of x-ray lines, the letters being shifted and broadened by the multiple ionization effects, were obtained in a restricted fitting procedure using the ionization probabilities for the M and N shells extracted from the measured L x rays. Moreover, the M-shell fluorescence and Coster-Kronig yields, used to obtain the M-subshell ionization cross sections from the measured x-ray production cross sections, were also modified for the multiple ionization effects. Consequently, in the present results on the M-shell ionization by oxygen ions the multiple ionization effects were accounted for systematically. The measured total M x-ray production cross sections are shown in Figs. 9–12, while the M-subshell ionization cross sections are presented in Figs. 15–18. The results are compared with the theoretical predictions of M-shell ionization using the PWBA, ECPSSR, ECUSAR, SCA-SA, SCA-UA, and BEA approaches discussed in Sec. VI.

The measured total M-shell ionization cross sections are in the best agreement ($\pm 20\%$) with the ECUSAR theory, clearly evidencing the improvement done in this approach with respect to the ECPSSR calculations which overestimate systematically the data, up to 30%. The predictions of the BEA approach reproduce qualitatively the energy trend in the data, but they overestimate the results for the higher energies. The SCA calculations within the united-atom limit (SCA-UA) are in good agreement with the low-energy data, while the high-energy points are systematically higher than calculated SCA-UA values, approaching the SCA-SA predictions.

The total M-shell ionization cross sections can be discussed in a universal manner in terms of the *reduced* M-shell ionization cross sections σ_M/σ_{M0}, where $\sigma_{M0} = 8\pi a_0^2 (Z_1^2/Z_{M_i}^4)$. According to the PWBA approach the reduced ionization cross sections scale with the dimensionless velocity parameter $\xi_M \propto v_1/v_{M_i}$ [see Eq. (9)] describing a dynamics of the ionization process. Such scaling of the ionization cross section with v_1/v_{M_i} is approximately valid for the SCA calculations, which gives a possibility to present M-shell data for different systems in a unified manner in order to compare them with the theoretical predictions. In Fig. 19 the reduced M-shell ionization cross sections for all measured elements are shown versus the scaled velocity ξ_M. These data are compared with the theoretical predictions of the PWBA, ECPSSR, ECUSAR, SCA, and BEA calculations. The scaled relative velocity ξ_M parameter separates the low- and high-energy regimes with $\xi_M < 1$ and $\xi_M > 1$, respectively. Consequently, Fig. 19 explains the agreement of the SCA-UA calculations with the data for low energies, for which small impact parameters dominate justifying the united-atom approximation. Similarly, the observed agreement between data and the SCA-SA calculations for high energies is due to the large impact parameters dominating the ionization process, which validates the separated-atoms approximation.

The measured M-subshell ionization cross sections for oxygen ion impact, shown in Figs. 15–18 for Au, Bi, Th, and U and in the form of a universal plot in Fig. 20, reveal the

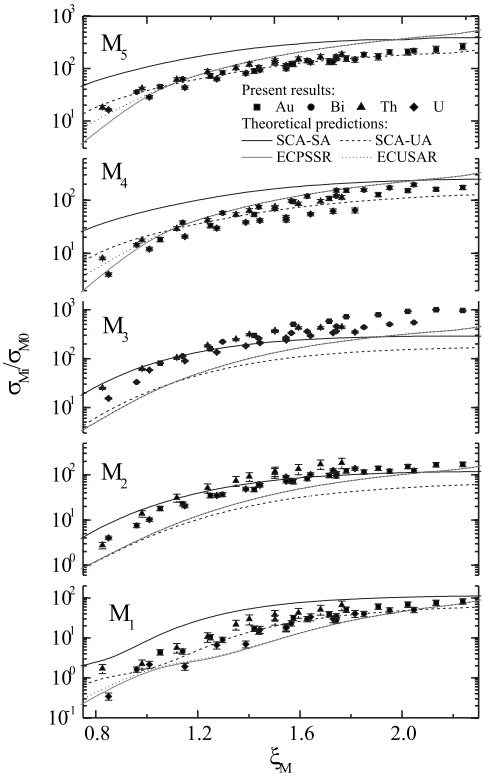

FIG. 20. The measured M-subshell ionization cross sections for oxygen ions in the energy range of 8.0–35.2 MeV plotted as the reduced ionization cross sections σ_M/σ_{M0} versus the scaled velocity parameter ξ_M for all studied elements. The experimental results are compared with the predictions of the ECPSSR, ECUSAR, and SCA calculations which are discussed in Sec. VI.

features, which were not accessible in the total M-shell ionization cross sections. Here, the M-subshell ionization cross sections for M_1-, M_4- and M_5 subshells, i.e., involving $3s_{1/2}$ and $3d_{3/2,5/2}$ electrons, agree quite well ($\pm 20\%$) with the SCA-UA calculations (with exception of M_1-subshell data for thorium), while the ECUSAR and ECPSSR predictions seem to be too low for M_1 subshell and too high for $M_{4,5}$ subshells for high energies. For the $M_{2,3}$ subshells ($3p_{1/2,3/2}$ electrons) the measured ionization cross sections are found to be substantially higher than theoretical predictions discussed. This effect could be, in our opinion, related to the subshell couplings, which are not treated in the present theoretical approaches. As other possible explanation, a modification of $M_{2,3}$ decay rates going beyond the treatment of this effect used in the present paper can be considered. These effects, however, need further studies in the future. Finally, the present results demonstrate that a rather good agreement of the ECUSAR/ECPSSR and BEA predictions with the total M-shell ionization cross section is not observed for the M-subshell ionization data, which are better described by the SCA-UA calculations using relativistic hydrogenic wave functions. This observation evidences the importance of the relativistic description of the electronic wave functions for the M shell.

VIII. CONCLUSIONS

The emission of M x rays from heavy Au, Bi, Th, and U atoms bombarded by oxygen ions in the energy range 8.0–35.2 MeV was studied systematically in order to investigate the M-shell ionization by heavy ions ($Z_1 \gg 1$) in asymmetric ($Z_1 \ll Z_2$) collision for which the direct Coulomb ionization dominates. The data were interpreted taking into account the multiple ionization affecting the measured x-ray spectra and M-shell fluorescence and Coster-Kronig yields relating the x-ray production and ionization cross sections. The measured ionization cross sections for the M shell were compared with theoretical predictions based on the PWBA, SCA, and BEA approximations. In particular, the electron binding effect was studied in more detail to investigate its description between the SA and UA limits. In this context the SCA-SA, SCA-UA, ECPSSR, and ECUSAR approaches were compared systematically with the data. Generally, the ECUSAR and ECPSSR theories reproduce the measured *total* M-shell ionization data reasonably well. In contrast, the experimental *M-subshell* ionization cross sections for M_1 and $M_{4,5}$ subshells ($3s$ and $3d$ electrons) are better described by the SCA-UA calculations, with exception of the $M_{2,3}$ subshells ($3p$ electrons) for which the data are systematically higher than the theoretical predictions. This effect, in our opinion, needs further investigations related to a role of the M-subshell couplings effect in ionization and the modifications of $3p$-vacancy decay rates in multiply ionized atoms. Finally, we would like to point out that the present measurements of the M-subshell ionization cross sections revealed important aspects concerning theoretical description of the ionization process in the M shell, which were not accessible interpreting the total M-shell ionization.

ACKNOWLEDGMENT

We would like to express our thanks to the staff of the Van de Graaff accelerator at the Institute of Physics, University of Erlangen-Nürnberg, for their contribution to this work.

[1] W. Bambynek, B. Crasemann, R. Fink, H.-U. Freund, H. Mark, C. Swift, R. Price, and P. V. Rao, Rev. Mod. Phys. **44**, 716 (1972).
[2] J. Garcia, R. Fortner, and T. Kavanagh, Rev. Mod. Phys. **45**, 111 (1973).
[3] C. H. Rutledge and R. L. Watson, At. Data Nucl. Data Tables **12**, 195 (1973).
[4] T. L. Hardt and R. L. Watson, At. Data Nucl. Data Tables **17**, 107 (1976).
[5] R. K. Gardner and T. J. Gray, At. Data Nucl. Data Tables **21**, 515 (1978).
[6] R. S. Sokhi and D. Crumpton, At. Data Nucl. Data Tables **30**, 49 (1984).
[7] H. Paul and J. Muhr, Phys. Rep. **135**, 47 (1986).
[8] G. Lapicki, J. Phys. Chem. Ref. Data **18**, 111 (1989).
[9] I. Orlić, C. H. Sow, and S. M. Tang, At. Data Nucl. Data

Tables **56**, 159 (1994).
[10] M. Pajek, A. P. Kobzev, R. Sandrik, R. A. Ilkhamov, and S. H. Khusmurodov, Nucl. Instrum. Methods Phys. Res. B **42**, 346 (1989).
[11] M. Pajek, A. P. Kobzev, R. Sandrik, A. V. Skrypnik, R. A. Ilkhamov, S. H. Khusmurodov, and G. Lapicki, Phys. Rev. A **42**, 261 (1990).
[12] M. Pajek, A. P. Kobzev, R. Sandrik, A. V. Skrypnik, R. A. Ilkhamov, S. H. Khusmurodov, and G. Lapicki, Phys. Rev. A **42**, 5298 (1990).
[13] M. Pajek, A. P. Kobzev, R. Sandrik, A. V. Skrypnik, R. A. Ilkhamov, S. H. Khusmurodov, and G. Lapicki, Phys. Rev. A **42**, 6582 (1990).
[14] A. Bieńkowski, J. Braziewicz, T. Czyżewski, L. Głowacka, M. Jaskóła, G. Lapicki, and M. Pajek, Nucl. Instrum. Methods Phys. Res. B **49**, 19 (1990).
[15] M. Pajek, M. Jaskóła, T. Czyżewski, L. Głowacka, D. Banaś, J. Braziewicz, W. Kretschmer, G. Lapicki, and D. Trautmann, Nucl. Instrum. Methods Phys. Res. B **150**, 33 (1999).
[16] M. Jaskóła, T. Czyżewski, L. Głowacka, D. Banaś, J. Braziewicz, M. Pajek, W. Kretschmer, G. Lapicki, and D. Trautmann, Nucl. Instrum. Methods Phys. Res. B **161-163**, 191 (2000).
[17] M. Pajek, D. Banaś, J. Braziewicz, M. Czarnota, A. Bieńkowski, M. Jaskóła, A. Korman, D. Trautmann, and G. Lapicki, Phys. Rev. A **73**, 012709 (2006).
[18] R. Mehta, J. L. Duggan, F. D. McDaniel, M. C. Andrews, G. Lapicki, P. D. Miller, L. A. Rayburn, and A. R. Zander, Phys. Rev. A **28**, 2722 (1983).
[19] M. C. Andrews, F. D. McDaniel, J. L. Duggan, P. D. Miller, P. L. Pepmiller, H. F. Krause, T. M. Rosseel, L. A. Rayburn, R. Mehta, and G. Lapicki, Phys. Rev. A **36**, 3699 (1987).
[20] J. L. Price, J. L. Duggan, F. D. McDaniel, G. Lapicki, and R. Mehta, Phys. Rev. A **37**, 365 (1988).
[21] Y. C. Yu, H. L. Sun, J. L. Duggan, F. D. McDaniel, J. Y. Jin, and G. Lapicki, Phys. Rev. A **52**, 3836 (1995).
[22] T. Czyżewski *et al.*, Nucl. Instrum. Methods Phys. Res. B **109-110**, 52 (1996).
[23] D. Mitra, M. Sarkar, D. Bhattacharya, P. Sen, and G. Kuri, Nucl. Instrum. Methods Phys. Res. B **145**, 283 (1998).
[24] Y. Singh and L. C. Tribedi, Phys. Rev. A **66**, 062709 (2002).
[25] Y. P. Singh, D. Misra, U. Kadhane, and L. C. Tribedi, Phys. Rev. A **73**, 032712 (2006).
[26] R. Merzbacher and H. W. Lewis, *Handbuch der Physik*, edited by S. Flügge (Springer, Berlin, 1958), Vol. 34.
[27] J. Bang and J. M. Hansteen, K. Dan. Vidensk. Selsk. Mat. Fys. Medd. **31**, No. 13 (1959).
[28] J. Garcia, Phys. Rev. A **1**, 280 (1970); **1**, 1402 (1970).
[29] J. McGuire and P. Richard, Phys. Rev. A **8**, 1374 (1973)
[30] W. Brandt and G. Lapicki, Phys. Rev. A **23**, 1717 (1981).
[31] G. Lapicki, G. A. V. Ramana Murty, G. J. Naga Raju, B. S. Reddy, S. B. Reddy, and V. Vijayan, Phys. Rev. A **70**, 062718 (2004).
[32] H. Paul and O. Bolik, At. Data Nucl. Data Tables **54**, 75 (1993).
[33] E. Huttel, W. Arnold, H. Baumgart, and G. Clausnitzer, Nucl. Instrum. Methods Phys. Res. B **12**, 193 (1985).
[34] D. Banaś, J. Braziewicz, U. Majewska, M. Pajek, J. Semaniak, T. Czyżewski, M. Jaskóła, W. Kretschmer, and T. Mukoyama, Nucl. Instrum. Methods Phys. Res. B **154**, 247 (1999).
[35] D. Banaś, J. Braziewicz, U. Majewska, M. Pajek, J. Semaniak, T. Czyżewski, M. Jaskóła, W. Kretschmer, T. Mukoyama, and D. Trautmann, J. Phys. B **33**, L793 (2000).
[36] F. Parente, M. H. Chen, B. Crasemann, and H. Mark, At. Data Nucl. Data Tables **26**, 383 (1981).
[37] W. Uchai, C. W. Nestor Jr., S. Raman, and C. R. Vane, At. Data Nucl. Data Tables **34**, 201 (1986).
[38] D. Banaś, M. Pajek, J. Semaniak, J. Braziewicz, A. Kubala-Kukuś, U. Majewska, T. Czyżewski, M. Jaskóła, W. Kretschmer, T. Mukoyama, and D. Trautmann, Nucl. Instrum. Methods Phys. Res. B **195**, 233 (2002).
[39] M. Czarnota *et al.*, Radiat. Phys. Chem. **68**, 121 (2003).
[40] M. Pajek *et al.*, Phys. Rev. A **68**, 022705 (2003).
[41] F. P. Larkins, J. Phys. B **4**, L29 (1971).
[42] M. H. Chen, B. Crasemann, K. N. Huang, M. Aoyagi, and H. Mark, At. Data Nucl. Data Tables **19**, 97 (1977).
[43] E. J. McGuire, Phys. Rev. A **5**, 1043 (1972).
[44] J. Oppenheimer, Phys. Rev. **31**, 349 (1928).
[45] H. Brinkmann and H. Kramers, Proc. K. Ned. Akad. Wet. **33**, 973 (1930).
[46] V. S. Nikolaev, Zh. Eksp. Teor. Fiz. **51**, 1263 (1966). Sov. Phys. JETP **24**, 847 (1967).
[47] G. Lapicki and F. D. McDaniel, Phys. Rev. A **22**, 1896 (1980).
[48] M. Born and J. Oppenheimer, Ann. Phys. **389**, 457 (1927).
[49] U. Fano and W. Lichten, Phys. Rev. Lett. **14**, 627 (1965).
[50] M. Barat and W. Lichten, Phys. Rev. A **6**, 211 (1972).
[51] J. Briggs, J. Phys. B **8**, L485 (1975).
[52] J. Briggs, Rep. Prog. Phys. **39**, 217 (1976).
[53] W. Lichten, J. Phys. Chem. **84**, 2102 (1980).
[54] U. Wille and R. Hippler, Phys. Rep. **132**, 129 (1986).
[55] A. Migdal, J. Phys. (USSR) **4**, 449 (1941).
[56] M. Kleber and K. Unterseer, Z. Phys. A **292**, 311 (1979).
[57] F. Rösel, D. Trautmann, and G. Baur, Nucl. Instrum. Methods Phys. Res. **192**, 43 (1982).
[58] D. Trautmann, F. Rösel, and G. Baur, Nucl. Instrum. Methods Phys. Res. **214**, 21 (1983).
[59] H. Bethe, Ann. Phys. **397**, 325 (1930).
[60] D. E. Johnson, G. Basbas, and F. D. McDaniel, At. Data Nucl. Data Tables **24**, 1 (1979).
[61] W. Brandt and G. Lapicki, Phys. Rev. A **20**, 465 (1979).
[62] E. Montenegro and A. de Pinho, J. Phys. B **15**, L275 (1982).
[63] N. Bohr, K. Dan. Vidensk. Selsk. Mat. Fys. Medd. **18**, No. 8 (1948).
[64] J. M. Hansteen, O. M. Johnsen, and L. Kocbach, At. Data Nucl. Data Tables **15**, 305 (1975).
[65] J. M. Hansteen and O. P. Mosebekk, Nucl. Phys. A. **201**, 541 (1973).
[66] J. M. Hansteen, Adv. At. Mol. Phys. **11**, 299 (1975).
[67] L. Kocbach, J. Phys. B **9**, 2269 (1976).
[68] Z. Halabuka, W. Preger, and D. Trautmann, Z. Phys. D: At., Mol. Clusters **29**, 151 (1994).
[69] J. J. Thomson, Philos. Mag. **23**, 449 (1912).
[70] M. Gryziński, Phys. Rev. **138**, A305 (1965); **138**, A322 (1965); **138**, A336 (1965).
[71] E. Gerjuoy, Phys. Rev. **148**, 54 (1966).
[72] L. Vriens, Proc. Phys. Soc. **90**, 935 (1967).
[73] J. Garcia, E. Gerjuoy, and J. Welker, Phys. Rev. **165**, 66 (1968).
[74] J. S. Hansen, Phys. Rev. A **8**, 822 (1973).
[75] V. Fock, Z. Phys. **98**, 145 (1935).